

Characteristic X-ray spectral variations in the iron L-band of IRAS 13224-3089, 1H0707-495 and NGC 4051

Misaki Mizumoto (JAXA/ISAS, Univ. of Tokyo)

Ken Ebisawa (JAXA/ISAS), Hiroaki Sameshima (Kyoto Sangyo Univ.),
Hiroki Yamasaki (JAXA/ISAS)

RMS spectra (Yamasaki, MM et al. 2016 PASJ)

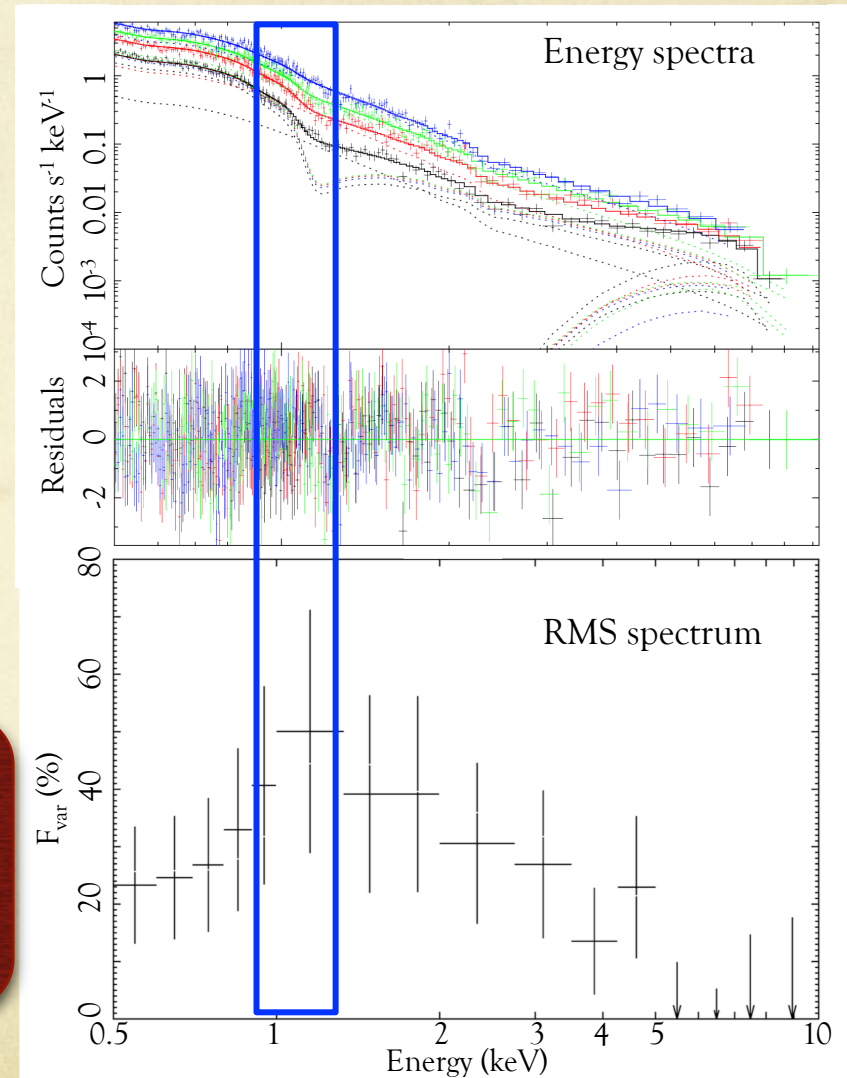
- Root-mean-square (RMS) spectrum

$$F_{\text{var}} = \frac{1}{\langle X \rangle} \sqrt{S^2 - \langle \sigma_{\text{err}}^2 \rangle}$$

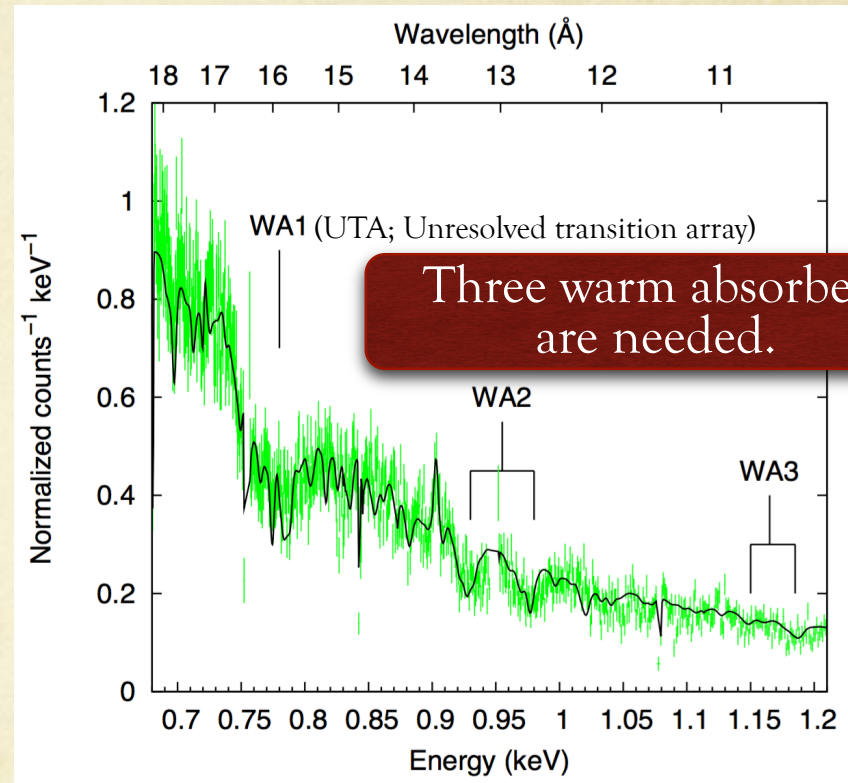
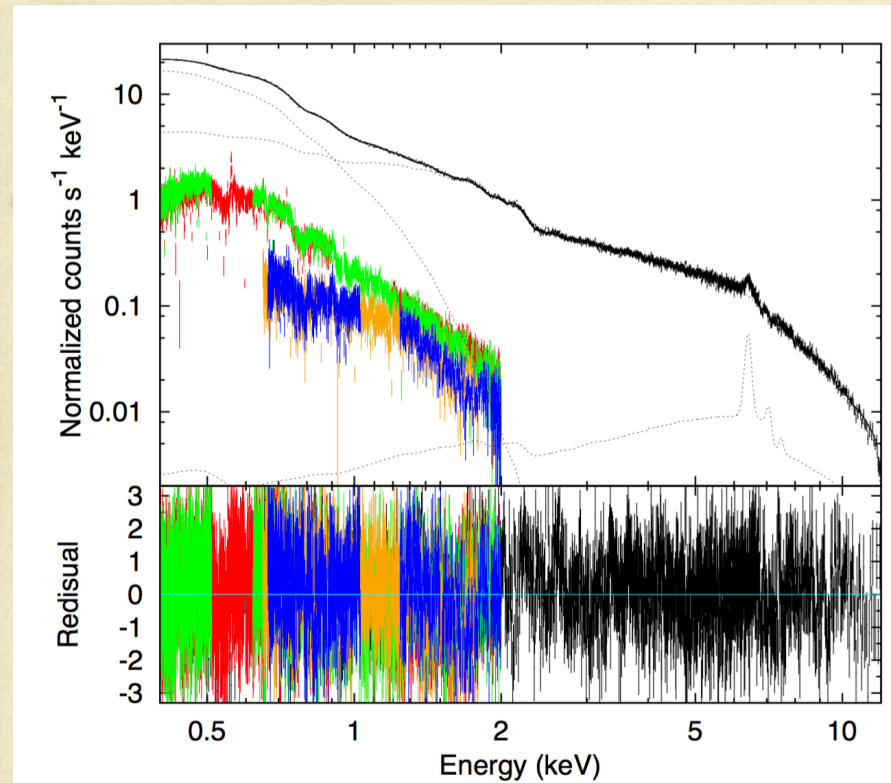
where $\langle X \rangle$ is the mean count rate,
 S^2 is the variance of the light curve,
 $\langle \sigma_{\text{err}}^2 \rangle$ is the mean error squared.

- IRAS 13224-3809
 - strong iron K- and L-edges

A strong RMS feature is seen at the Fe-L energy band.



NGC 4051 (MM, Ebisawa 2016, submitted)

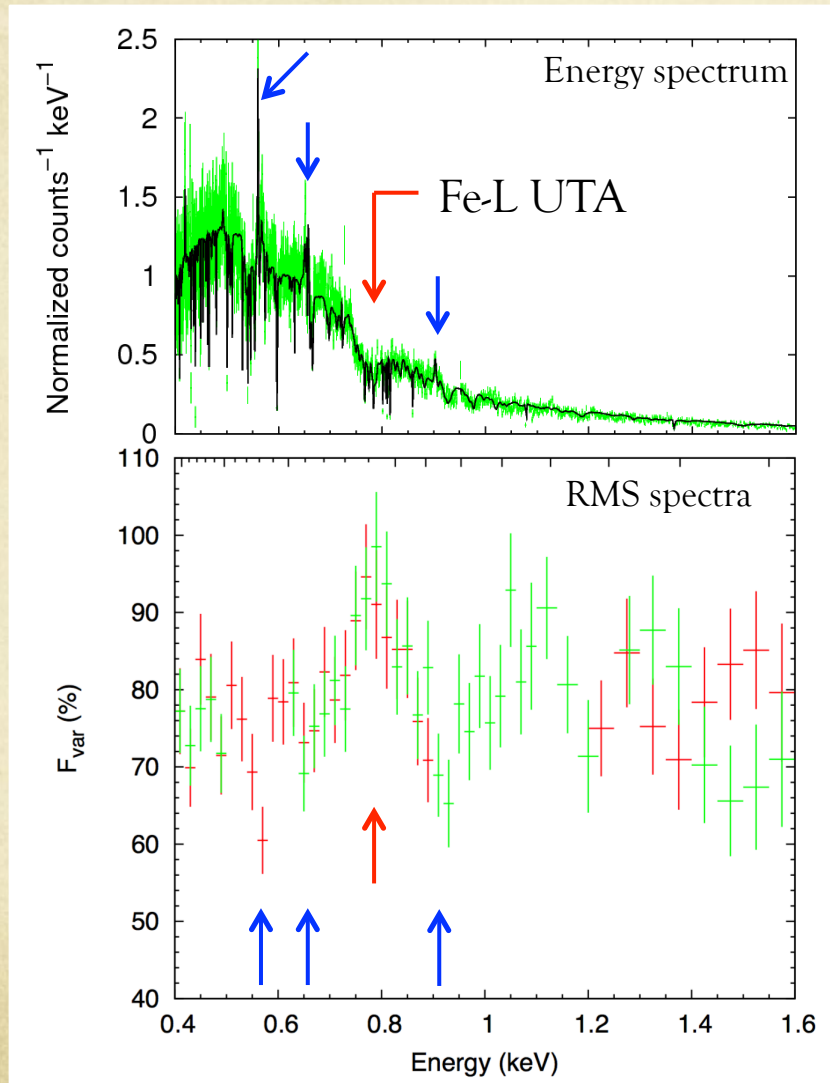


- Long exposure (600ks XMM observation in 2009)
- Strong Fe-L absorption feature
→ Best target
- $T_{\text{babs}} \times \{(\text{MCD} + \text{PL}) \times \text{WA1} \times \text{WA2} \times \text{WA3} + \text{reflection}\}$

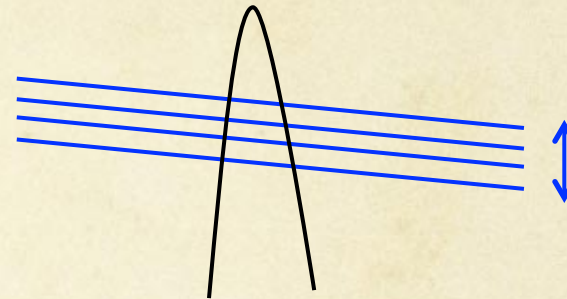
	N_{H} (cm^{-2})	$\log \xi$	v (km/s)
WA1	2.5×10^{21}	1.5	-650
WA2	8.7×10^{21}	2.5	-4000
WA3	6.7×10^{23}	3.4	-6100

RMS spectra

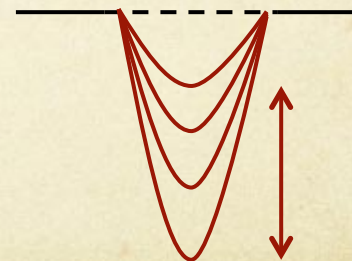
NGC4051



Non-variable emission lines
-> RMS dips

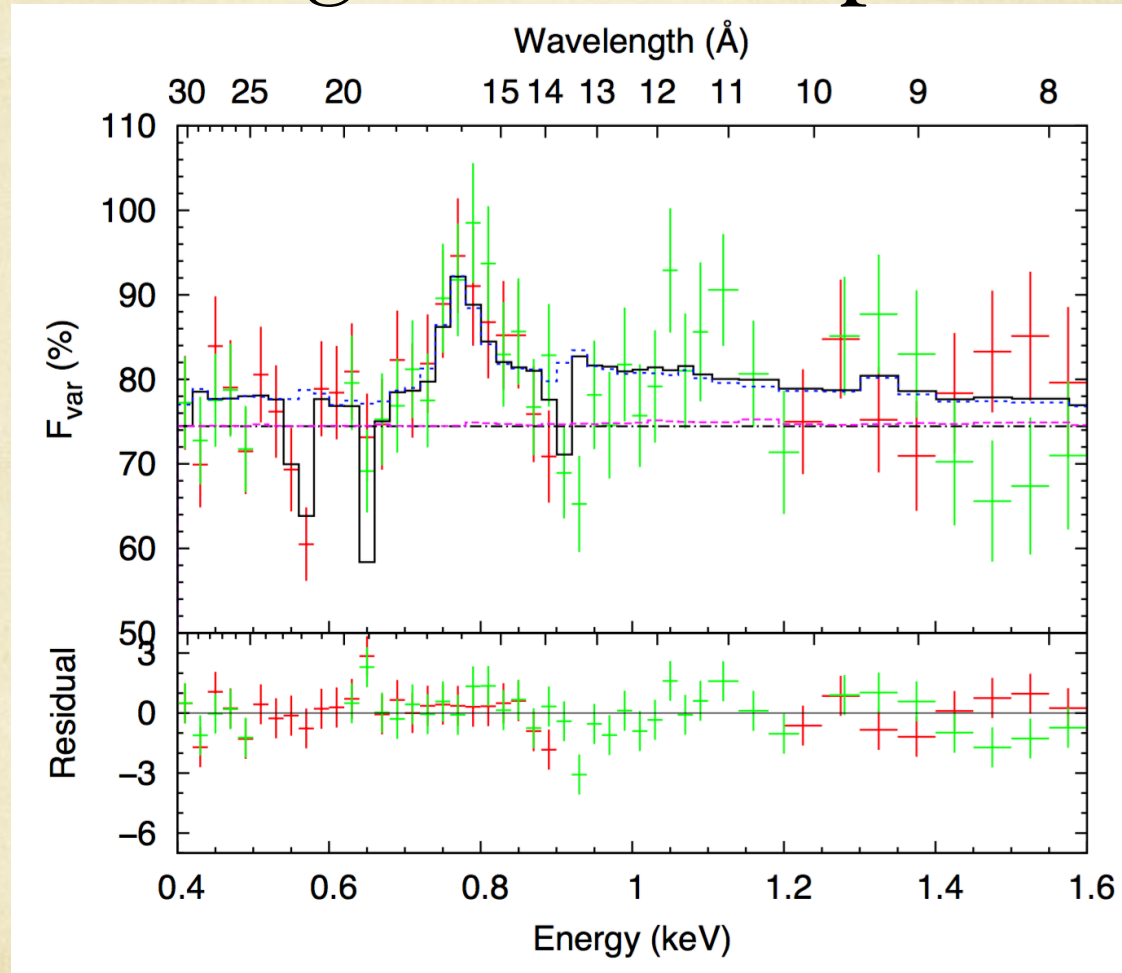


Variable absorption lines
-> RMS peaks



Fe-L UTA is variable.

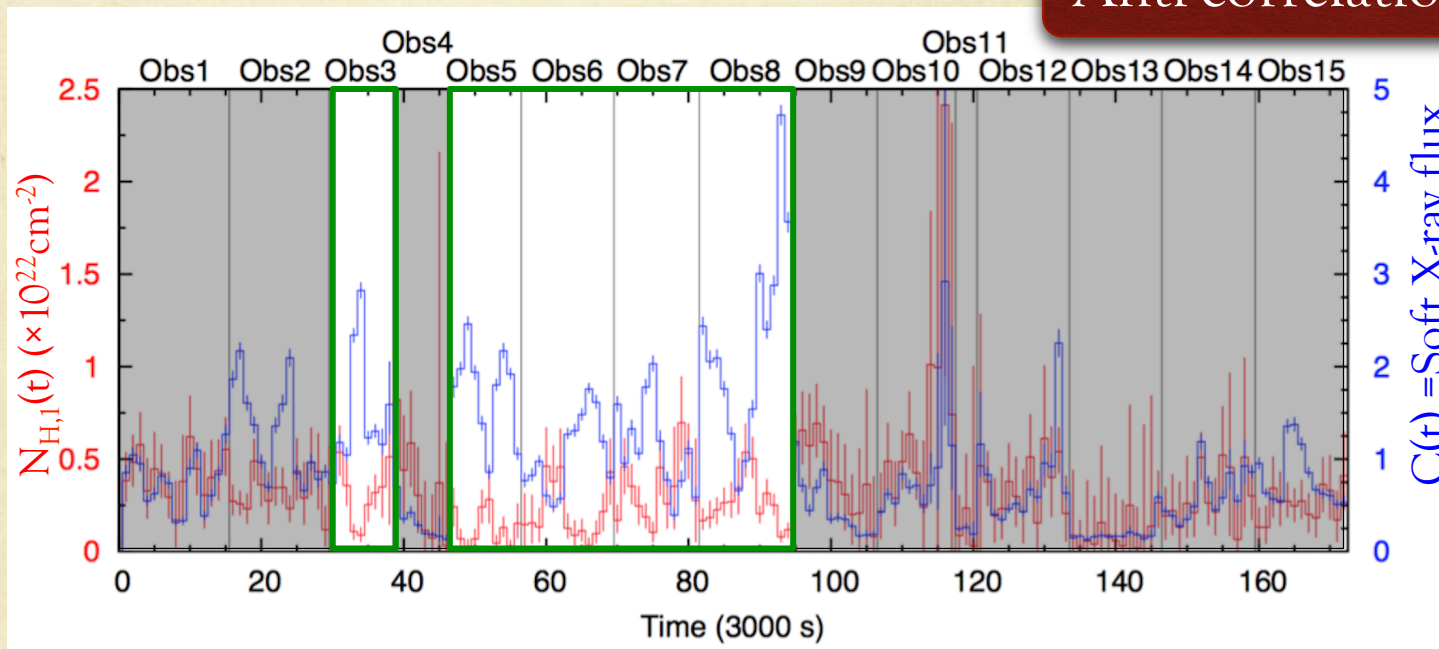
Fitting of RMS spectra



Only WA1 is variable,
whereas WA2, 3 are not variable.

Time variations

Anti-correlation



Create time-sliced spectra of RGS (< 2 keV) with 3000s, and fit them with

$$T_{\text{babs}}(E) \times \{(\text{MCD}(E) + \text{PL}(E)) \times C(t) \times \text{WA1}(E, t) \times \text{WA2}(E) \times \text{WA3}(E) + \text{Reflection}(E)\}$$

- $C(t)$: Variation of the continuum (= Variation of the soft X-ray flux)
- $\text{WA1}(E, t) = \exp[-\sigma_1(E)N_{\text{H},1}(t)]$

Interpretation of the model

$$T_{\text{babs}}(E) \times \{(\text{MCD}(E) + \text{PL}(E)) \times C(t) \times \text{WA1}(E, t) \times \text{WA2}(E) \times \text{WA3}(E) + \text{Reflection}(E)\}$$

Variation of soft X-ray flux
 → Partial covering of Compton-thick clouds (W_{thick})
 (e.g. Pounds et al. 2004, Lobban et al. 2011)

$$C(t) = 1 - \alpha(t) \\ = 1 - \alpha(t) + \alpha(t) \frac{W_{\text{thick}}(E)}{W_{\text{thick}}(E)} \\ (=0 \text{ when } E < 2 \text{ keV})$$

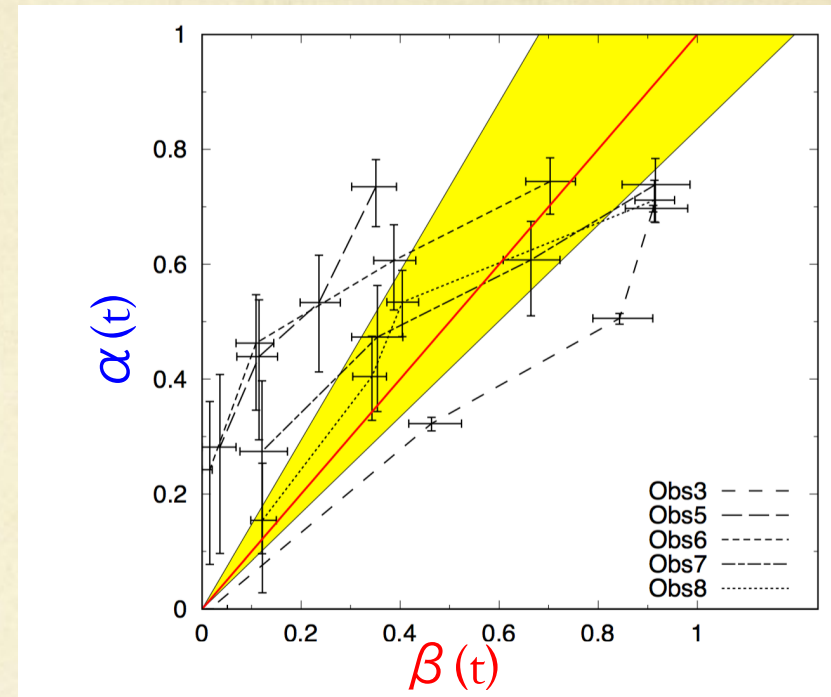
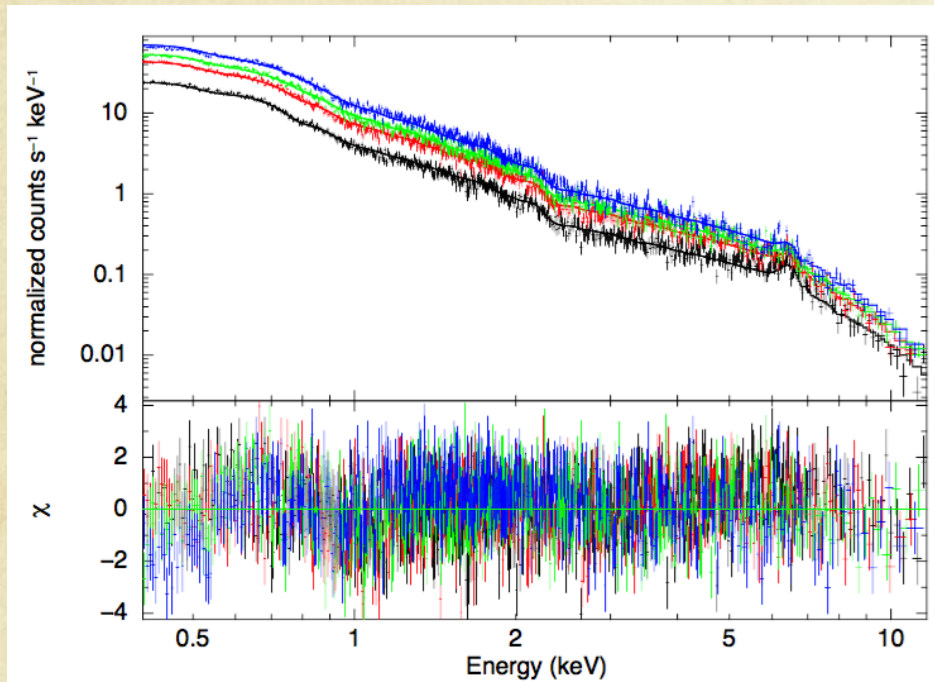
Variation of N_{H} of WA1
 → Partial covering of optically-thin clouds
 (Mizumoto et al. 2014)

$$\text{WA1}(E, t) \\ = \exp[-\sigma_1(E)N_{\text{H},1}(t)] \\ \approx 1 - \sigma_1(E)N_{\text{H},1}(t) \quad (\text{when } \sigma N_{\text{H}} \ll 1) \\ = 1 - \sigma_1(E)\beta(t)N_{\text{H},1}^{\text{fixed}} \\ = 1 - \beta(t) + \beta(t)(1 - \sigma_1(E)N_{\text{H},1}^{\text{fixed}}) \\ \approx 1 - \beta(t) + \beta(t)\exp[-\sigma_1(E)N_{\text{H},1}^{\text{fixed}}] \\ = 1 - \beta(t) + \beta(t)\text{WA1}(E)$$

Double partial covering

$$T_{\text{babs}}(E) \times \{(\text{MCD}(E) + \text{PL}(E)) \times (1 - \alpha(t) + \alpha(t)W_{\text{thick}}(E)) \\ \times (1 - \beta(t) + \beta(t)\text{WA1}(E)) \times \text{WA2}(E) \times \text{WA3}(E) + \text{Reflection}(E)\}$$

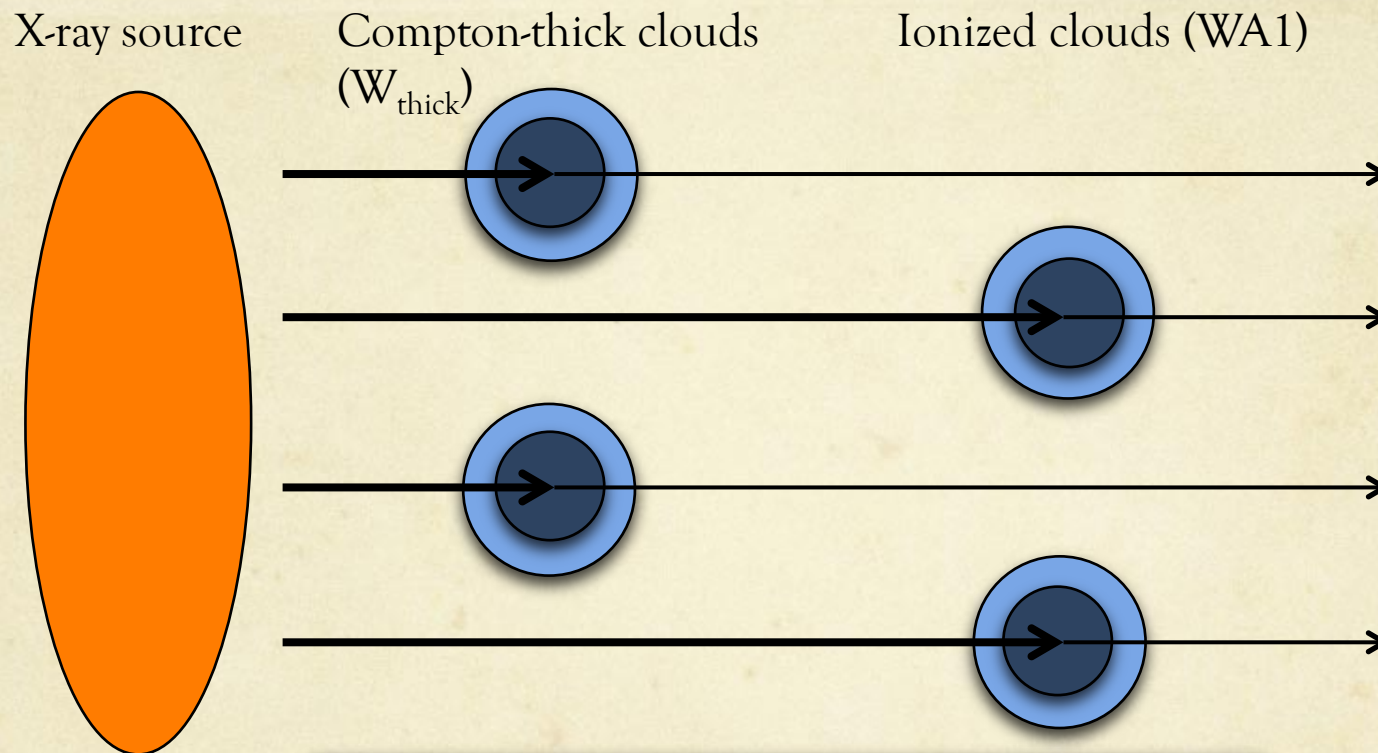
Intensity-sliced spectra



$$T_{\text{babs}}(E) \times \{ (MCD(E) + PL(E)) \times (1 - \alpha(t) + \alpha(t) W_{\text{thick}}(E)) \times (1 - \beta(t) + \beta(t) WA1(E)) \times WA2(E) \times WA3(E) + \text{Reflection}(E) \}$$

The two partial covering fractions are equal.

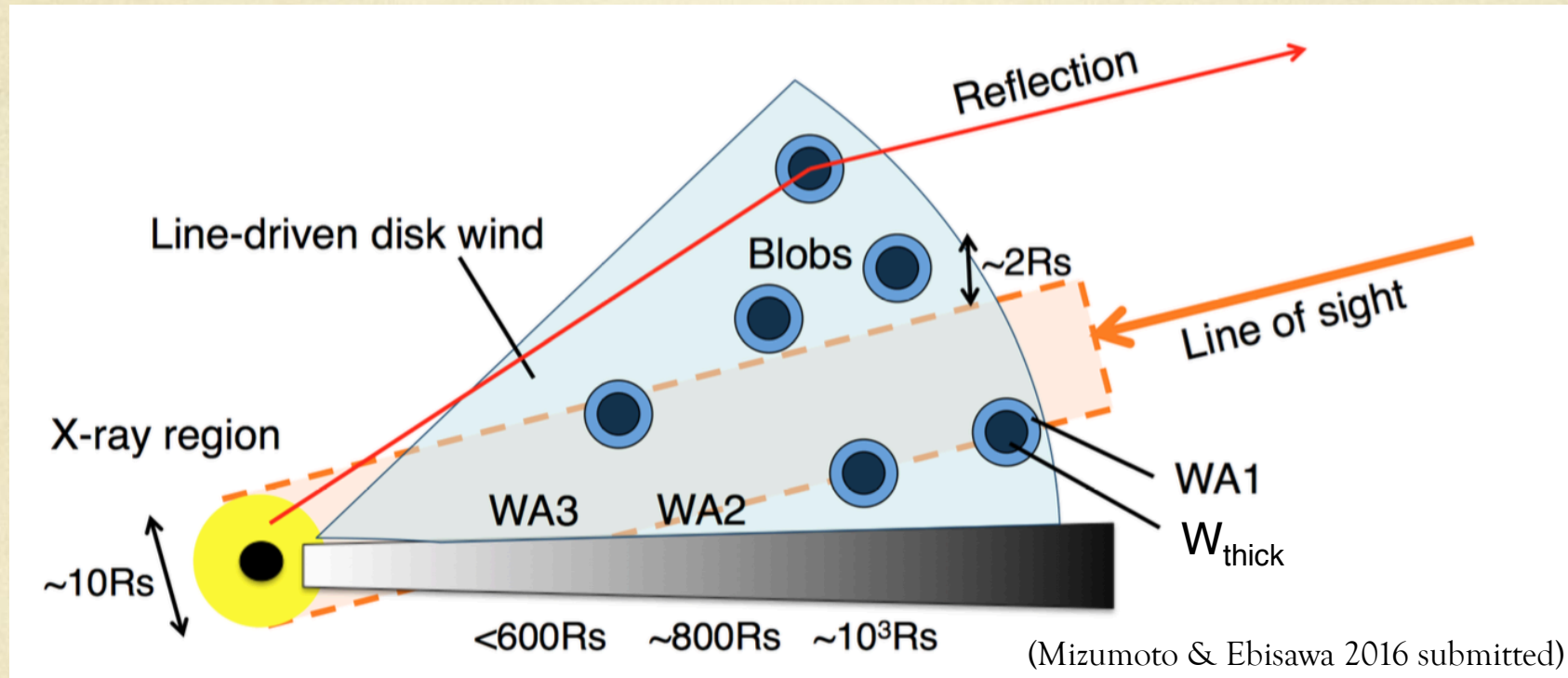
Double partial covering



Partial covering fractions are equal.

Partial covering of double-layer clouds

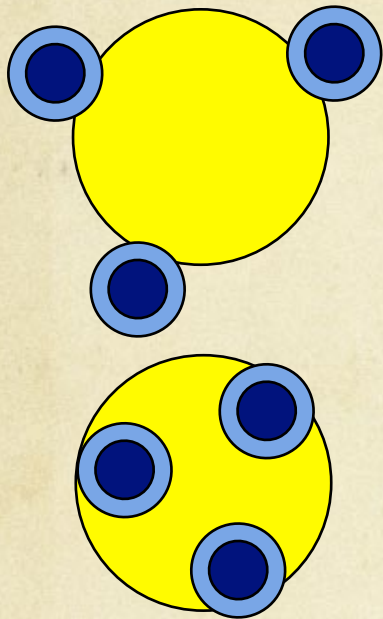
Geometry of WAs in NGC 4051



WA1 and W_{thick} create
partial covering clouds with double-layer
(Dusty wind?)

WA2,3 show no variability
→ extended in the line of sight

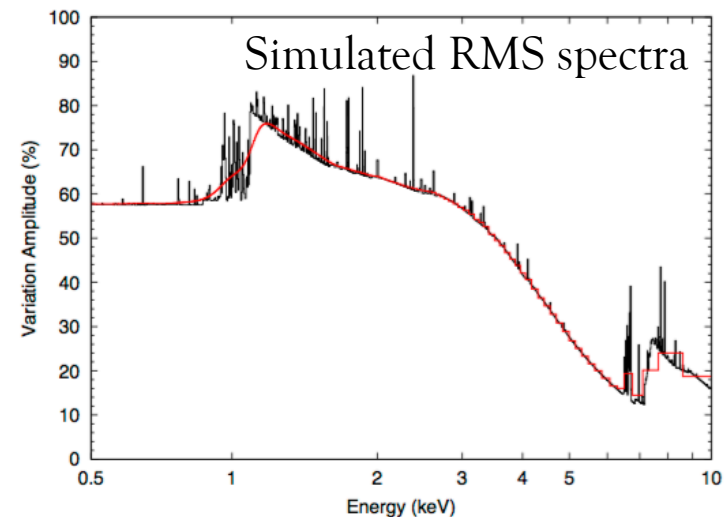
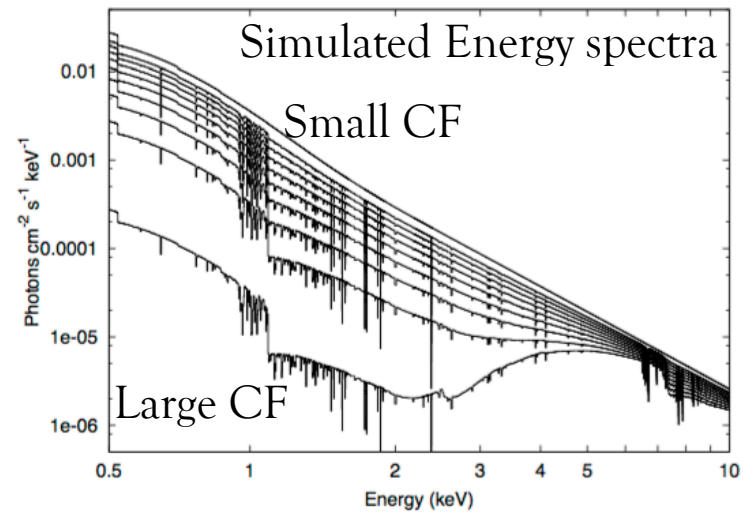
RMS peaks of IRAS 13224 and 1H0707



Small covering fraction
→ Bright X-ray flux
Weak Fe-L edge

Large covering fraction
→ Faint X-ray flux
Strong Fe-L edge

Partial covering of double-layer clouds can explain the RMS spectra



IRAS13224 (Yamasaki, MM, et al. 2016)